

ANTIPROTON PRODUCTION AND ACCUMULATION *

V. Lebedev[#], FNAL, Batavia, IL 60510, U.S.A.

Abstract

In the course of Tevatron Run II (2001-2007) improvements of antiproton production have been one of major contributors to collider luminosity growth. Commissioning of Recycler ring in 2004 and making electron cooling operational in 2005 freed Antiproton source from the necessity to keep large stacks in the Accumulator and allowed us to boost the antiproton production. That resulted in doubling average antiproton production during last two years. The paper discusses improvements and upgrades of the Antiproton source during last two years and future developments aimed at further stacking improvements.

INTRODUCTION

Improvements in the Tevatron resulted in that the fraction of antiprotons burned in collisions achieved ~40% in 2004. Since that time this number was not changed, and its further increase is limited by intrabeam scattering (IBS) in the proton and antiproton beams. Further growth of the collider luminosity would not be possible without growth of antiproton production. For past two years increased antiproton production has been our highest priority in Tevatron Run II. Figure 1 demonstrates the results of these efforts culminating in ~1.7 times antiproton production growth in FY'07 alone. Further growth is expected in FY'08.

The following items contributed to this growth of antiproton production. First, there has been an improvement of the proton source. A reduction of longitudinal emittance in the Booster allowed us to optimize slip-stacking in the Main injector [1], which resulted in an increase in the number of protons on the antiproton production target from $6.5 \cdot 10^{12}$ to $8 \cdot 10^{12}$ per pulse. Second, an optics correction in the transfer line from the Main Injector to the antiproton production target allowed us to reduce the rms beam size on the target to ~200 μm . The resulting increased target depletion rate limits further reduction of the beam size. Third, stabilization of the proton beam position on the antiproton production target resulted in more stable operation and ~5% growth in the average antiproton production (it did not change the peak production). Fourth, an upgrade of the lithium lens allowed us to increase its gradient from 60 to 75 kG/cm, which resulted in ~10% growth in the antiproton yield. Fifth, optics correction in the Debuncher [2] resulted in an increase in Debuncher acceptance from 30/25 to 35/34 mm mrad, correspondingly for horizontal and vertical degrees of freedom. This resulted in ~10% improvement of the antiproton yield.

After the above upgrades were finished by the end of FY'06 the remaining major limitation to the stacking rate

was the Stacktail system. Therefore its improvement became the highest priority item for the last year. This project combines a few separate improvements that are described in detail below. The implementation of these improvements resulted in a growth of peak stacking rate from $20 \cdot 10^{10}$ to $23.2 \cdot 10^{10}$ hour⁻¹ in FY'07 and positioned us well for further improvements of stacking rate. Figure 2 shows how the dependence of stacking rate on stack size has changed during the course of Run II. As one can see, the stacking rate drops fast with the stack size. To minimize this harmful effect the transfer time from Accumulator to MI injector was decreased from ~50 to 9 min. That allowed us to reduce the maximum stack size to ~ $50 \cdot 10^{10}$ and greatly decrease the difference between the peak and average stacking rates. This resulted in the best average weekly stacking rate of $16.5 \cdot 10^{10}$ hour⁻¹, which is only ~28% below the peak stacking rate. This number looks quite impressive if one takes into account that it also includes all interruptions to the stacking.

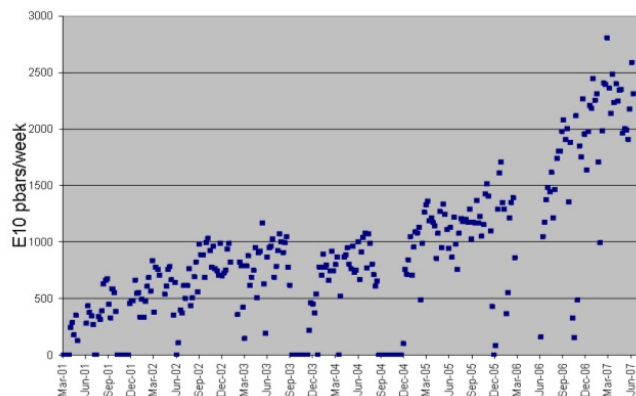


Figure 1: Weekly antiproton production rate during Run II (2001-2007).

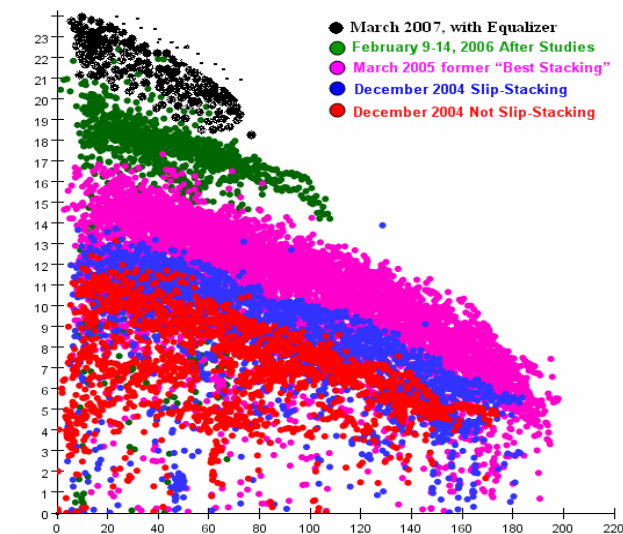


Figure 2: Dependence of antiproton production rate (units of 10^{10} hour⁻¹) on stack size (units of 10^{10}) during Run II.

* Work supported by Fermi Research Alliance, LLC., under contract DE-AC02-76CH03000 with the U.S. Dept. of Energy.
[#] val@fnal.gov

The upgrade of the Stacktail system [3] has also included a few other systems which are logically connected to Stacktail operation. It has consisted of a few steps. First, we optimized tuning of the existing system. This included a large increase of the gain for 4-8 GHz longitudinal core cooling system (February 2006). There was also a polarity flip for the Stacktail amplifier (October 2006). That corrected the phase intercept and, consequently, increased the bandwidth. Second, we corrected phase and magnitude of the system gain by installation an equalizer [4, 5]. An equalizer prototype was installed in March of 2007 and the final equalizer was installed in June 2007. The equalizer increased the bandwidth of the Stacktail, which resulted in faster stacking but also caused stronger transverse and longitudinal heating of the core. Third, the transverse heating was mitigated by an Accumulator optics correction [6]. That increased the slip factor and resulted in less heating (see below). If unaddressed the slip factor increase would also result in a larger phase variation of the gain on the way from the deposition orbit to the core orbit. To reduce this phase variation we moved the pickups of legs 2 and 3 closer to the leg 1 pickups and began using leg 3 pickups¹. Fourth, to mitigate the longitudinal heating we replaced one of three Stacktail BAW (bulk acoustic wave) notch filters by the superconducting notch filter, and we will install the equalizer for the longitudinal 4-8 GHz core cooling system by the end of the 2007 shutdown (October 2007).

STACKTAIL MODEL

Improvements of the stacktail system would not be possible without its detailed model. The model is based on the beam measurements [4] and includes all the important features of the system.

Evolution of the beam longitudinal distribution is described by the Fokker-Planck equation [6]:

$$\frac{\partial f}{\partial t} + \frac{\partial}{\partial x}(F(x)\psi) = \frac{1}{2} \frac{\partial}{\partial x} \left(D(x) \frac{\partial \psi}{\partial x} \right), \quad (1)$$

where $x = \Delta p/p$ is the relative momentum deviation, $\psi(x)$ is the distribution function ($\int \psi(x) dx = N$), N is the number of particles in the beam,

$$F(x) = f_0 \sum_{n=-\infty}^{\infty} \frac{G_{tot}(x, \omega_n)}{\varepsilon(\omega_n)} \exp(i\omega_n T_2 \eta_2 x) \quad (2)$$

is the cooling force,

$$D(x) = f_0 \psi(x) \sum_{n=-\infty}^{\infty} \frac{1}{n\eta} \frac{1}{|\varepsilon(\omega_n)|^2} |G_{tot}(x, \omega_n)|^2 \quad (3)$$

describes the diffusion due to the beam noise, f_0 is the revolution frequency, $\omega_n = 2\pi f_0(1 - \eta x)n$, η is the slip factor, T_2 is the pickup-to-kicker travel time, η_2 is the partial pickup-to-kicker slip factor, and $\varepsilon(\omega)$ is the beam dielectric permeability. The Stacktail system has a sufficiently large signal-to-noise ratio allowing us to neglect diffusion due to noise of electronics.

¹ Only Legs 1 and 2 were used before this modification

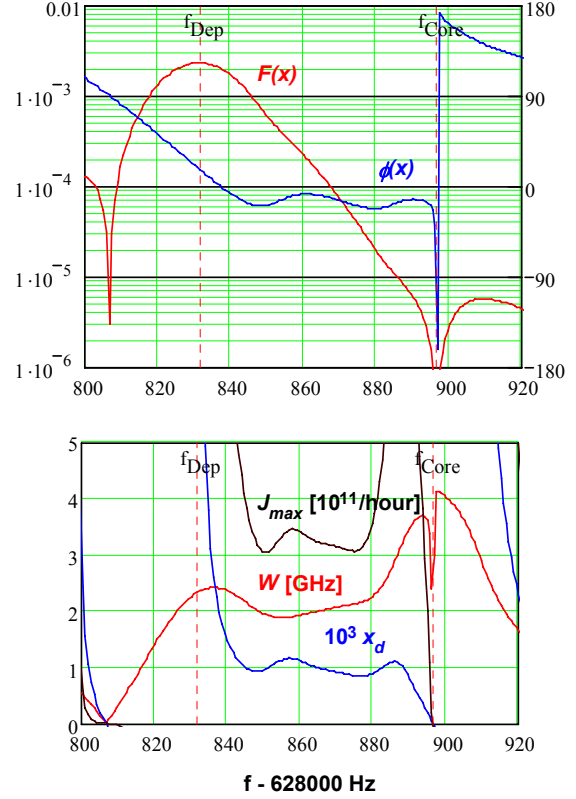


Figure 3: Dependence of Stacktail parameters on the revolution frequency; top: red line – cooling force, blue line – phase of the cooling force; bottom: red line – effective bandwidth, blue line – x_d , black line – maximum flux computed using Eq. (7).

The total gain of the system is combined from the gains of three pickup systems (legs 1, 2 & 3) belonging to the Stacktail system and two core systems (2-4 GHz and 4-8 GHz). Each leg is centered on its own momentum, and the gains and delays for each leg are independently controlled. The block diagram of the Stacktail system is presented in Figure 2 of Ref. [4]. The corresponding total gain can be presented in the following form

$$G_1(x, \omega) = K_{24}(\omega)G_{24}(x, x_{core}) + K_{48}(\omega)G_{48}(x, x_{core}) + (1 - A_3(\omega)e^{-i\omega T_{03}}) \{ K_1(\omega)G_1(x, x_1) [1 - A_1(\omega)e^{-i\omega T_{01}}] + [K_2(\omega)G_2(x, x_2) + K_3(\omega)G_3(x, x_3)] [1 - A_2(\omega)e^{-i\omega T_{02}}] \}. \quad (4)$$

Here terms in the parenthesis describe the effect of notch filters, $K_k(\omega)$ and $K_{xx}(\omega)$ are the electronics gains, and $G_k(\dots)$ and $G_{xx}(\dots)$ are the space gains of Stacktail and core systems, correspondingly. The space gain of each leg is parameterized as following:

$$G_k(x, x_k) = (1/\pi) \left[\text{atan}(\sinh((\pi/h_k)(x - x_k + w_k/2))) - \text{atan}(\sinh((\pi/h_k)(x - x_k - w_k/2))) \right], \quad k = 1, 2, 3. \quad (5)$$

where h_k and w_k are the effective gaps and widths of pickups, and x_k are the positions of pickup centers. Each of the core cooling systems consists of two pickups with design similar to the stacktail pickups. These pickups are located on the different sides of the core orbit and are wired in difference mode. Their space gains are presented

as difference of two terms. Each term is given by Eq. (5) but the terms have opposite sign offsets relative to the core orbit. Table 1 presents the parameters for all pickups. Parameter A presents relative gains of different pickups at their maximum sensitivities. In normal operating conditions the ratios for the Stacktail legs are fixed while the core cooling gains are changed with beam current.

Table 1: Parameters of Stacktail pickups

	X [cm]	W [cm]	H [cm]	A
Leg 1	0.97	3	3.2	1
Leg 2	-0.29	3	3	0.34
Leg 3	-2	3	3	0.023
Core 2-4 GHz	-3.45/-8.42	2	2.7	$2 \cdot 10^{-3}$
Core 2-4 GHz	-5.06/-6.58	0.76	3.2	$1.6 \cdot 10^{-3}$

Eq. (5) describes well the beam based measurements in the entire stacktail region (see Figures 5 and 6 in Ref. [4]). The only exception is the Leg 1 response on the core orbit, where the Leg 1 pickup sensitivity at the high frequency end is ~ 2 times higher than predictions of Eq. (5). Taking into account that the Leg 1 sensitivity at the core orbit is ~ 50 dB smaller than at its center, and that it contributes to the gain at the core orbit less than other two legs, this complication was neglected in the model.

As was proved in Ref. [7] the notch filter terms have to be outside the integral in the dielectric permeability calculation. This results in:

$$\varepsilon(\omega) = 1 + (1 - A_3(\omega)e^{-i\omega t_{03}}) \left\{ \left(1 - A_1(\omega)e^{-i\omega t_{01}} \right) \int_{\delta \rightarrow 0_+} \frac{d\psi(x)}{dx} \frac{K_1(\omega)G_1(x, x_1)e^{i\omega t_2 \eta_2 x}}{e^{i\omega t_0(1+\eta x)} - (1-\delta)} dx + (1 - A_2(\omega)e^{-i\omega t_{02}}) \int_{\delta \rightarrow 0_+} \frac{d\psi(x)}{dx} \frac{K_2(\omega)G_2(x, x_2) + K_3(\omega)G_3(x, x_3)}{e^{i\omega t_0(1+\eta x)} - (1-\delta)} e^{i\omega t_2 \eta_2 x} dx \right\} + \int_{\delta \rightarrow 0_+} \frac{d\psi(x)}{dx} \frac{K_{24}(\omega)G_{24}(x, x_{core}) + K_{48}(\omega)G_{48}(x, x_{core})}{e^{i\omega t_0(1+\eta x)} - (1-\delta)} e^{i\omega t_2 \eta_2 x} dx. \quad (6)$$

The system optimization has been based on a static solution of Eq. (1) in Van der Myer approximation. That results in the maximum flux:

$$J_{\max}(x) = |\eta| W(x)^2 x_d(x) / f_0, \quad (7)$$

where

$$W(x) = \sqrt{\left(\int_0^\infty \operatorname{Re}(G_{tot}(x, 2\pi f)) df \right)^2 / \int_0^\infty |G_{tot}(x, 2\pi f)|^2 \frac{df}{f}} \quad (8)$$

is the effective bandwidth, and $x_d(x) = F(dF/dx)^{-1}$ is the inverse rate of the relative gain change. Parameters of the system were adjusted to maximize the total flux with an approximately constant $x_d(x)$ in the central part of the Stacktail, which for a given flux maximizes the gain difference between the deposition and core orbits. Figure 3 presents the results of calculations with this static model after all upgrades. One can see that the cooling force achieves its maximum at the deposition orbit and then exponentially decays in direction of the core orbit with $p x_d \approx 9$ MeV. It approaches zero at the core due to notch filters which minimize heating of the core by Stacktail.

Because the addends in Eq. (2) for positive and negative n are complex conjugates of one other, $F(x)$ is a real function. To compute the phase of the cooling force, ϕ , we compute the sum in Eq. (2) for positive n only and denote the result as F_p ; then $F = 2\operatorname{Re}(F_p)$ and $\exp(i\phi) = F_p / |F_p|$. The effective bandwidth is changing through the Stacktail due to the notch filters. It starts at ~ 2.4 GHz at the deposition orbit, slightly decreases and then goes up to ~ 4 GHz in at the core where the 4-8 GHz core cooling system dominates. The static model predicts maximum stacking rate of $\sim 30 \cdot 10^{10} \text{ hour}^{-1}$.

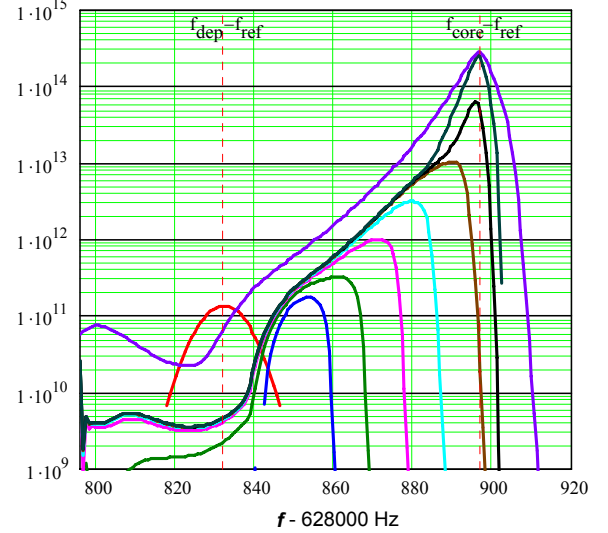


Figure 4: Results of stacking simulations for the system after all upgrades; $2 \cdot 10^8$ antiprotons are injected every 2.4 s; red line – distribution function after injection of the first antiproton pulse, other lines present distributions just before injection of pulses with numbers: 2, 4, 11, 31, 101, 301, 1001, 2001, 3001.

After system parameters were optimized Eq. (1) was solved numerically. The results of the calculations are presented in Figure 4. One can see that at the beginning the Stacktail pushes particles to the core. Then the core starts to be formed after ~ 20 min (core size $\sim 10 \cdot 10^{10}$); and finally the core becomes too large and back-streaming starts at the core size of $\sim 25 \cdot 10^{10}$ antiprotons (1 hour after stacking start). The simulations predict the same stacking rate of $\sim 30 \cdot 10^{10} \text{ hour}^{-1}$ as the static model described above. Nevertheless, in addition to the limitation of Eq. (7), there appears to be another effect which can limit the stacking rate. It is the deposition orbit clearing requiring the Stacktail to remove antiprotons from the deposition area before the next injection happens. As one can see from the stack evolution the deposition orbit clearing and the stacktail throughput of Eq. (7) are well balanced for the parameters of the Accumulator Stacktail system.

To make an estimate of the deposition orbit clearing we ignore the dependence of the cooling force on momentum and assume that the gain is equal to zero outside of the band $[f_1, f_2]$ while it is set to its maximum value (limited by the beam stability) inside the band. For beam with a Gaussian distribution the maximum gain is:

$$G(\omega_n) = C_s \sigma^2 \eta m / N, \quad C_s \approx 9.011, \quad (9)$$

where σ is the rms relative momentum spread. Substitution of Eq. (9) into Eq. (2) results in:

$$F = C_s \frac{\sigma^2 \eta}{N} \frac{f_2^2 - f_1^2}{f_0} = 2C_s \frac{\sigma^2 \eta}{N} \frac{W^2}{f_0}, \quad (10)$$

where we took into account that $W = \sqrt{(f_2^2 - f_1^2)/2}$.

Requiring the distribution to be moved by distance $C_s \sigma$ ($C_s \approx 2.5$) during one stacking cycle ($F \Delta T = C_s \sigma$) one finally obtains a stacking rate estimate from the point of view of deposition orbit clearing:

$$J \approx \frac{C_s}{C_\sigma} \frac{f_2^2 - f_1^2}{f_0} \sigma \eta = \frac{2C_s}{C_\sigma} \frac{W^2}{f_0} \sigma \eta \approx 6 \frac{W^2}{f_0} \sigma \eta. \quad (11)$$

This estimate yields ~ 5 times larger result than the numerical solution described above because the distribution widening due to diffusion and the cooling force drop at the distribution edges (3 times at 2.5σ) were neglected. Eq. (11) yields that if the stacking rate is limited by the deposition orbit clearing it can be mitigated by an increase of σ . Nevertheless this requires larger power which is not always available. Taking into account that in the case of Accumulator the fluxes of Eqs. (7) and (11) are well balanced; that both of them are proportional to the slip factor; that the operation of stacktail system is power limited; and that the stacking rate increase by the slip factor increase does not change the stacktail power we increased η by 15% from 0.0131 to 0.015 [6]. Further increase is limited by the band overlap and by variation of the cooling force phase through the stacktail region.

Before the equalizer installation the model predicted a peak stacking rate of $\sim 22 \cdot 10^{10}$ hour⁻¹, which is close to the experimental value. Nevertheless after the equalizer installation the stacking rate grew to only $\sim 24 \cdot 10^{10}$ hour⁻¹ instead of the expected $\sim 30 \cdot 10^{10}$ hour⁻¹. The stacking rate has been limited by strong transverse and longitudinal core heating excited by stacktail operation. This heating limits the stacktail power to about half of the pre-equalizer operation (0.9 kW instead of 1.8 kW). A few steps were made to mitigate this. First results are already seen and more improvements are expected in the future.

TRANSVERSE CORE HEATING

There are two major sources of core heating due to stacktail operation. The first one is a consequence of non-zero dispersion at the stacktail kickers; and the second one is related to the quadrupole kicks excited together with longitudinal kick due to the finite size of the pickup loops. Stacktail kickers have similar design and geometry to the stacktail pickups and therefore in accordance with the reciprocity theorem [8] the longitudinal kick and the pickup sensitivity depend similarly on the transverse coordinate. Expanding Eq. (5) in Taylor series one obtains the dependence of longitudinal kick on the particle transverse coordinates:

$$U(X, Y) = U_0 \left(1 + \kappa (X^2 - Y^2) / 2a_{eff}^2 \right) + \dots \quad (12)$$

Here $\kappa = \pm 1$ with signs “+” and “-“ assigned to the

kickers rolled so that in the difference mode they would be the horizontal or vertical kickers correspondingly, and the effective gap is

$$a_{eff} = \frac{h}{\pi} \cosh(\pi w / 2h) \sqrt{\frac{\text{atan}(\sinh(\pi w / 2h))}{\sinh(\pi w / 2h)}}. \quad (13)$$

$a_{eff} = 1.7$ cm for the Accumulator stack-tail kickers. In the case where the particle velocity, v_0 , coincides with the phase velocity of the kicker wave, the transverse and longitudinal kicks are related so that [8]:

$$\frac{\Delta p_x}{p} = \kappa \frac{iv_0}{\omega} \frac{\Delta p_x}{p} \frac{x}{a_{eff}^2}, \quad \frac{\Delta p_y}{p} = -\kappa \frac{iv_0}{\omega} \frac{\Delta p_x}{p} \frac{y}{a_{eff}^2}. \quad (14)$$

Each kicker tank has four kickers located in the same plane so that the higher order modes could be damped. To mitigate the kick non-uniformity each next kicker tank is rolled to the orthogonal plane.

The transverse kicks described above introduce two mechanisms for the emittance growth. The first one is related to offsets of kickers from the beam center resulting in the transverse kicks proportional to the kicker offset and, consequently, the emittance growth excited by noise on the betatron sidebands. The second mechanism is related to the quadrupole kicks. That result in the parametric excitation of betatron motion and, consequently, the emittance growth excited by sidebands of doubled betatron frequency. Comparatively straight forward calculations yield the following expression for the emittance growth rate excited by the stacktail:

$$\begin{aligned} \frac{d\varepsilon}{dt} \Big|_{param} &= \frac{d\varepsilon}{dt} \Big|_{dip} + \frac{d\varepsilon}{dt} \Big|_{param}, \\ \frac{d\varepsilon}{dt} \Big|_{dip} &= \frac{f_0 \beta_{kick}}{2} \sum_{k,m=-\infty}^{\infty} \frac{\psi(p_{km})}{|\eta k|} |G(p_{km}, \omega_{km})|^2 |D_{eff}(\omega_{km})|^2, \\ \frac{1}{\varepsilon} \frac{d\varepsilon}{dt} \Big|_{param} &= \frac{v_0^2 \beta_{eff}^2}{8\pi^2 f_0 a_{eff}^4} \sum_{k,m=-\infty}^{\infty} \frac{\psi(\tilde{x}_{km})}{|\eta k^3|} |G_{tot}(\tilde{x}_{km}, \tilde{\omega}_{km})|^2. \end{aligned} \quad (15)$$

Here $x_{km} = x - (v + m) / \eta k$, $\tilde{x}_{km} = x - (2v + m) / \eta k$,

$$\omega_{km} = \omega_0 (v + m + k(1 - \eta x)), \quad \tilde{\omega}_{km} = \omega_0 (2v + m + k(1 - \eta x))$$

are the resonant momenta and frequencies. The term,

$$D_{eff}(\omega) = \frac{v_0 \hat{X}(\omega)}{\omega a_{eff}^2} + \frac{D'_{kick} \beta_{kick} + \alpha_{kick} D_{kick} - i D_{kick}}{\beta_{kick}}, \quad (16)$$

accounts for the effective offset of kickers, $\hat{X}(\omega)$, and the finite value of the dispersion in the kicker section. Here β_{kick} , α_{kick} , D_{kick} , and D'_{kick} are the beta- and alpha-functions, the dispersion and the dispersion prime in the kicker section center. The positions of kicker electrical centers, $X_i(\omega)$, depend on frequency resulting in the frequency dependence of the effective offset:

$$\hat{X}(\omega) = \left(\sum_{i=1}^{N_{kick}} \kappa_i X_i(\omega) + \frac{\alpha_{kick} - i}{\beta_{kick}} \sum_{i=1}^{N_{kick}} \kappa_i s_i X_i(\omega) \right) / \sum_{i=1}^{N_{kick}} |\kappa_i|, \quad (17)$$

where s_i is the longitudinal coordinate of the i -th kicker relative to the kicker section center. The effective beta-function of the parametric excitation is equal to:

$$\beta_{eff}^2 = \frac{1}{N_{kick}^2} \sum_{i,j=1}^{N_{kick}} \kappa_i \kappa_j \left(\beta_0^2 + 2s'_i s'_j + \frac{s_i^2 s_j'^2}{\beta_0^2} - (s'_i - s'_j)^2 \right), \quad (18)$$

where s'_i is the longitudinal coordinate of i -th kicker relative to the location of beta-function minimum, β_0 .

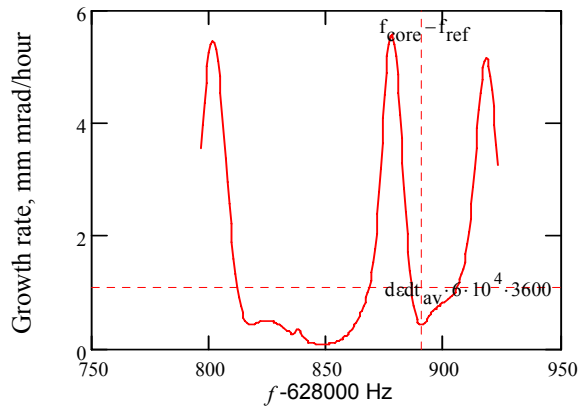


Figure 5: Dependence of transverse heating rate on the revolution frequency before Accumulator optics upgrade. Horizontal line marks the heating rate averaged over particle distribution.

Table 2: Heating and cooling rates at normal operation

Heating mechanisms	mm mrad/hour
IBS heating at 50 mA	~3
Stacktail heating	5-6
Noise of core systems	~2
Total heating = Total cooling	~10

Table 3: Estimate of Stacktail heating

Heating mechanisms	mm mrad/hour
Parametric heating	~0.25
Dispersion mismatch	~2.4
Kicker offset (res. at 3.25 GHz)	~1.2 - 2.2
Unaccounted (most probably due to geometric kicker offset)	~1.1 mm

The Stacktail system uses 8 kicker tanks located close to each other in one straight section. Each tank has four kickers. One of these 32 kickers is used for the longitudinal core cooling other 31 for the stacktail. It has become apparent that parametric heating has been a problem for a long time. The problem was resolved after two kickers on each side of kicker straight section were switched off. That reduced the effective beta-function of the parametric heating, β_{eff} , from 2.3 to 0.6 m resulting in negligible parametric heating. After the equalizer installation we observed the strong transverse heating again. This time it was excited by a resonance in the kickers which became much more apparent with the increased bandwidth. The resonance occurs at 3.25 GHz and results in a resonant displacement of kicker electrical center with frequency. The amplitude of the displacement is ~2 mm and the quality factor is ~27. Figure 5 presents dependence of computed horizontal heating rate on the revolution frequency. Tables 2 and 3 present measured heating and cooling rates for the horizontal degree of freedom before the optics upgrade.

The optics upgrade increased the slip factor and resulted in the displacement of heating peaks (related to

lower and upper betatron sidebands) so that the core became better centered between the peaks. That reduced the heating. In addition it reduced IBS and improved the core cooling resulting in acceptable values for transverse emittances.

PLANS

The following upgrades will be introduced after the 2007 shutdown end in the first half of October. First, the upgrade of Debuncher transverse and longitudinal cooling systems should improve their cooling times by about 10%. Second, a Debuncher optics correction should improve vertical cooling by additional 5%. Third, an improved equalizer will be installed into 4-8 GHz core cooling systems resulting in more than a 50% improvement in its damping rate. Fourth, faster Accumulator-to-Recycler transfers will allow us to reduce the stack size, which should additionally mitigate transverse and longitudinal heatings. Together with a few other operational improvements we expect the average stacking rate be above $20 \cdot 10^{10}$ /hour by the next summer.

ACKNOWLEDGMENTS

The author would like to thank A. Burov for multiple discussions devoted to the stochastic cooling theory and K. Gollwitzer, V. Nagaslaev, R. Pasquinelli, D. Sun, S. Werkema, D. Vander Meulen as well as the entire Antiproton source department for help in measurements, data analysis and operational support of the Antiproton source. Without their work and devotion this work could not happen.

REFERENCES

- [1] K. Seiya, *et. al.*, "Multi-batch Slip Stacking in the Main Injector at Fermilab," PAC-2007, p. 742.
- [2] V.P. Nagaslaev, *et. al.*, "Measurement and Optimization of the Lattice Functions in the Debuncher Ring at Fermilab," EPAC-2006, p. 2050.
- [3] R. Pasquinelli, D. McGinnis, "Performance of the Upgraded Stacktail Momentum Cooling System in the Fermilab Antiproton Source," Proceedings of the 1993 Part. Accel. Conference, p. 2361-2363
- [4] R. Pasquinelli, V. Lebedev, S. Werkema, "Beam Based measurements for Stochastic Cooling Systems at Fermilab," This conference.
- [5] D. Sun, *et. el.*, "New Equalizer for Antiproton Stochastic Cooling at Fermilab at Fermilab," This conference.
- [6] V. Nagaslaev, *et. al.*, "Lattice Optimization for the Stochastic cooling in the Accumulator ring at Fermilab," This conference.
- [7] V. Lebedev, "Stochastic Cooling with Schottky Band Overlap," COOL'05, AIP Conf. proc., v. 821, p. 231.
- [8] J. Bisognano and C. Leemann, "Stochastic Cooling," 1981 Summer School on High Energy Particle Accelerators, AIP Conf. Proceedings, N. 87, New York, 1982, p.584.